

A Meshless Method for Solving the EEG Forward Problem

Nicolás von Ellenrieder*, *Student Member, IEEE*, Carlos H. Muravchik, *Senior Member, IEEE*, and Arye Nehorai, *Fellow, IEEE*

Abstract—We present a numerical method to solve the quasi-static Maxwell equations and compute the electroencephalography (EEG) forward problem solution. More generally, we develop a computationally efficient method to obtain the electric potential distribution generated by a source of electric activity inside a three-dimensional body of arbitrary shape and layers of different electric conductivities. The method needs only a set of nodes on the surface and inside the head, but not a mesh connecting the nodes. This represents an advantage over traditional methods like boundary elements or finite elements since the generation of the mesh is typically computationally intensive. The performance of the proposed method is compared with the boundary element method (BEM) by numerically solving some EEG forward problems examples. For a large number of nodes and the same precision, our method has lower computational load than BEM due to a faster convergence rate and to the sparsity of the linear system to be solved.

Index Terms—EEG, EEG forward problem, layered media, meshless method, moving least squares approximation, numerical solution, volume conductor.

I. INTRODUCTION

ESTIMATION of the intensity, location, and orientation of sources of neuronal activity in the brain from EEG signals has attracted much interest in neurology. These sources of activity generate an electric potential distribution in the head that is noninvasively measured with a suitable array of electrodes on the scalp. The computation of the electric potential distribution generated by current density sources with known parameters, i.e., known source intensity, orientation, and location, is the so-called EEG *forward* problem. Estimation of the source parameters based on the electric potential measurements is known as the EEG *inverse* problem. This paper essentially deals with the forward problem.

To get an accurate solution to the EEG forward problem it is necessary to correctly model the shape of the head and its elec-

tric properties [1]. A prevalent model consists on layers of different electric conductivities, constant within layers. The shape of the layers is obtained for example by magnetic resonance imaging (MRI) or X-ray tomography.

The irregular geometry of the head model requires the problem to be solved numerically. Frequently employed numerical techniques, such as boundary element method (BEM) or finite element method (FEM), require nodes on or inside the surfaces of the head layers, and a mesh partitioning the domain of the problem into a set of small two-dimensional (2-D) (BEM) or three-dimensional (3-D) (FEM) elements. A simple variation (constant or linear) is assumed for the electric potential over each element, and the resulting differential or integral equations are solved to get the potential at the nodes [1]–[5]. Very often spherical approximations to the head surfaces are used to reduce the computational load of these methods [6].

Once the geometry of the problem is known it is easy to select the locations of the nodes. But the generation of a mesh connecting them to define the elements is a more difficult, time-consuming job, especially for FEM. Although in BEM the mesh can be generated automatically [7], it still requires dedicated software and computing time. To overcome these complications, a method that uses only the locations of the surface points would be desired. A number of methods that do not require a mesh connecting the nodes have been developed for a wide range of applications [8]–[17]. In this paper, we present a meshless method for solving the EEG forward problem.

In Section II, we describe the head and source of brain electric activity models, and state the mathematical expression for the EEG forward problem. The proposed meshless method is described in detail in Section III, and some of its possible variations in Section IV. In Section V, we present some numerical results obtained with our method and compare the performance with the well-known BEM. Finally, in Section VI we discuss the results of the method and state the future work.

II. THE EEG FORWARD PROBLEM

In this section, we describe the head and source models and state the mathematical EEG forward problem. As is typical in EEG, the head is modeled as a body formed by nearly concentric layers Ω_i of different conductivities σ_i , constant within each layer, representing the tissues. The surfaces S_i between the i th and $(i + 1)$ th layers are assumed to be smooth. In the common three-layers model, they represent the brain, skull, and scalp, see Fig. 1. In general, M layers could be used for a more accurate representation of the head including cerebrospinal fluid, differences between gray and white matter, etc.

Manuscript received October 2, 2003; revised June 27, 2004. The work of N. von Ellenrieder was supported in part by the Consejo Nacional de Investigaciones Científicas y Técnicas (CONICET). The work of C. Muravchik was supported in part by the Comisión de Investigaciones Científicas de la Provincia de Buenos Aires (CICPBA). The work of A. Nehorai was supported in part by the National Science Foundation under Grant CCR-0105334 and Grant CCR-0330342. *Asterisk indicates corresponding author.*

*N. von Ellenrieder is with the Laboratorio de Electrónica Industrial, Control e Instrumentación, Departamento de Electrotecnia, Facultad de Ingeniería, Universidad Nacional de La Plata, C.C. 91, 1900 La Plata, Argentina (e-mail: nellen@ieee.org, ellenrie@ing.unlp.edu.ar).

C. H. Muravchik is with the Laboratorio de Electrónica Industrial, Control e Instrumentación, Departamento de Electrotecnia, Facultad de Ingeniería, Universidad Nacional de La Plata, 1900 La Plata, Argentina.

A. Nehorai is with the Department of Electrical and Computer Engineering, University of Illinois at Chicago, Chicago, IL 60608 USA.

Digital Object Identifier 10.1109/TBME.2004.840499

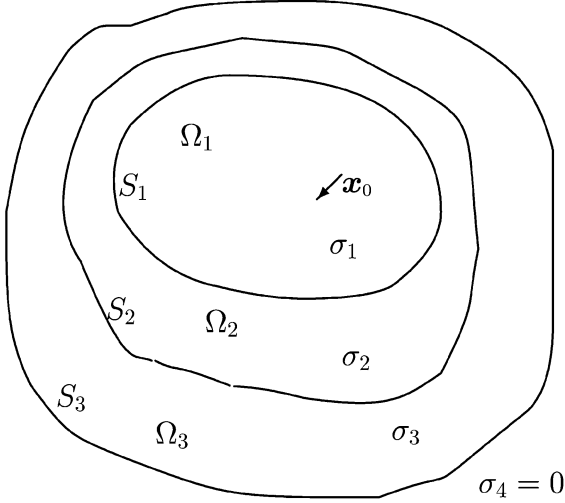


Fig. 1. Schematic electromagnetic model of the head. Concentric layers Ω_i of constant conductivities σ_i separated by smooth surfaces S_i , $i = 1, 2, 3$. An electric current dipole located at the point \mathbf{x}_0 is the source of activity.

A group of active neurons is a source of electric activity in the brain, and can be described in many instances of interest for EEG as an electric current dipole [18]. Let \mathbf{x}_0 and \mathbf{q} be the dipole position and moment (intensity q and orientation \mathbf{q}/q), respectively. Since the electric activity of the neurons takes place in the brain, the source will be located in the inner layers, i.e., $\mathbf{x}_0 \in \Omega_i$, usually with $i = 1$ or 2 . Hence the problem, in local or differential form, is the following:

$$\begin{cases} \sigma(\mathbf{x})\nabla^2\phi(\mathbf{x}) = \nabla \cdot (\mathbf{q}\delta(\mathbf{x} - \mathbf{x}_0)), & \mathbf{x} \in \Omega \\ \phi(\mathbf{x}^+) = \phi(\mathbf{x}^-), & \\ \sigma_i\nabla\phi(\mathbf{x}^-) \cdot \mathbf{n} = \sigma_{i+1}\nabla\phi(\mathbf{x}^+) \cdot \mathbf{n}, & \mathbf{x} \in S_i \end{cases} \quad (1)$$

where \mathbf{x} is any point in the domain $\Omega = \bigcup_{i=1}^M \Omega_i$, ∇^2 is the Laplacian operator and ∇ is the gradient operator. The electric potential at \mathbf{x} is $\phi(\mathbf{x})$, the electric conductivity of the layer where \mathbf{x} is located is $\sigma(\mathbf{x})$, and \mathbf{n} is the outward normal to the surface S_i . For any point $\mathbf{x} \in S_i$, $\mathbf{x}^- \in \Omega_i$ is the limit point of a spatial sequence inside S_i , and $\mathbf{x}^+ \in \Omega_{i+1}$ is the limit point of a spatial sequence outside S_i . Solving the forward problem using (1) is challenging due to spatially rapid variations of the mathematical expression for the electric potential in the neighborhood of a dipole, with values up to $\pm\infty$. Any numerical approximation to the analytic solution of the potential near this singularity will necessarily be very poor.

To avoid this difficulty it is possible to remove the singularity using the linearity of the Laplacian operator; this forward problem restatement has been used in FEM formulations [5]. By linearity, the electric potential can be found as the superposition of the two terms $\phi(\mathbf{x}) = \phi_F(\mathbf{x}) + \Phi(\mathbf{x})$, where each term is given by

$$\begin{cases} \sigma(\mathbf{x}_0)\nabla^2\phi_F(\mathbf{x}) = \nabla \cdot (\mathbf{q}\delta(\mathbf{x} - \mathbf{x}_0)), & \mathbf{x} \in \Omega \\ \sigma(\mathbf{x})\nabla^2\Phi(\mathbf{x}) = 0, & \mathbf{x} \in \Omega \\ \Phi(\mathbf{x}^-) = \Phi(\mathbf{x}^+), & \\ \sigma_i\nabla\Phi(\mathbf{x}^-) \cdot \mathbf{n} - \sigma_{i+1}\nabla\Phi(\mathbf{x}^+) \cdot \mathbf{n} & \mathbf{x} \in S_i \\ = (\sigma_{i+1} - \sigma_i)\nabla\phi_F(\mathbf{x}) \cdot \mathbf{n} & \end{cases} \quad (2)$$

The term $\phi_F(\mathbf{x})$ corresponds to the electric potential generated by a dipole source in an infinite homogeneous medium of conductivity $\sigma(\mathbf{x}_0)$. This term has a singularity since the electric potential is not defined at the dipole's position, but it presents no difficulty because it can be solved analytically, yielding the following expression:

$$\phi_F(\mathbf{x}) = \frac{1}{4\pi\sigma_1} \frac{(\mathbf{x} - \mathbf{x}_0)}{|\mathbf{x} - \mathbf{x}_0|^3} \cdot \mathbf{q}. \quad (4)$$

The term $\Phi(\mathbf{x})$ in (3) corresponds to a Laplace equation with Neumann boundary conditions [19], and must be computed numerically because it is related to the irregular geometry of the head model. All the information regarding the source in this term is present in the boundary conditions, as can be seen in (3). This term has no singularity, so its solution is smoother than the solution of the original problem, improving the accuracy of any numerical approximation. Of course, there is an unavoidable numerical difficulty when the dipole source is very close to an interface.

From now on this procedure will be referred to as the singularity separation method (SSM). The finite points mixed method (FPMM) presented in the Section III will be used for solving the numerical part of the SSM, i.e., the solution for $\Phi(\mathbf{x})$.

III. FINITE POINTS MIXED METHOD

We propose a FPMM that uses a collocation technique to discretize the governing equation(3). The electric potential is replaced by a global approximation written as a linear combination of shape functions, each one of them associated to one node. The coefficients of this global approximation are chosen to solve the discretized EEG forward problem. The shape functions result from building a *moving least squares* local approximation to the electric potential about the nodes in terms of a basis of simple functions. The method is said to be mixed because the solution satisfies exactly neither the differential equation in the domain nor the boundary conditions [20].

First, we show how to obtain the shape functions that will be used to construct the global approximation of the electric potential, then we explain how the forward problem is solved by computing the coefficients of the global approximation, which we will call Φ . The moving least squares approximation is a standard procedure in many meshless methods, e.g., [17], but we include it here to introduce the notation and our choice of local basis and weight functions.

Consider a set of nodes \mathbf{x}_j in the domain Ω_i and on the surface $\partial\Omega_i = S_i \cup S_{i-1}$, of any layer $i = 1, \dots, M$, $S_0 \triangleq \emptyset$. The component $\Phi(\mathbf{x})$ of the electric potential is approximated in the neighborhood of any point $\mathbf{x} \in \Omega_i$ assuming a simple variation

$$\Phi(\mathbf{x}) \approx \Phi^a(\mathbf{x}) = \sum_{k=1}^K p_k(\mathbf{x})a_k = \mathbf{p}^T(\mathbf{x})\mathbf{a} \quad (5)$$

where $\Phi^a(\mathbf{x})$ is the electric potential approximation, $\mathbf{p}(\mathbf{x})$ is the vector of K functions of the approximation basis. In this paper, we choose a complete monomial basis of order 2 with $K = 10$ elements, in three dimensions $\mathbf{x} = (x, y, z)$, and the basis is

$$\mathbf{p}(x, y, z) = [1, x, y, z, xy, xz, yz, x^2, y^2, z^2]^T. \quad (6)$$

There exist a certain number N of nodes \mathbf{x}_j around \mathbf{x} . Let $\tilde{\Phi}_j = \Phi(\mathbf{x}_j)$ be the value of the electric potential on the nodes $j = 1, \dots, N$. We will show that this potentials $\tilde{\Phi}_j$ are the coefficients of a global approximation of the electric potential. To do this we must relate the vector \mathbf{a} in (5), which contains the coefficients of the local approximation, to the potentials $\tilde{\Phi}_j$. The vector \mathbf{a} associated with the point \mathbf{x} is obtained then by minimizing the functional

$$J(\mathbf{x}) = \sum_{j=1}^N w_j(\mathbf{x})(\tilde{\Phi}_j - \mathbf{p}^T(\mathbf{x}_j)\mathbf{a})^2 \quad (7)$$

i.e., $J(\mathbf{x})$ is the sum of the weighted approximation errors to the potentials $\tilde{\Phi}_j$ on the nodes $j = 1, \dots, N$.

The weight function $w_j(\mathbf{x})$ associated with the node $j = 1, \dots, N$, evaluated at \mathbf{x} , is responsible for the local character of the approximation. The support of the weight function, also known as the influence region of the j th node, is a spherical region centered at \mathbf{x}_j with radius r_j . In this way, for a given \mathbf{x} , the size of the r_j of nodes near \mathbf{x} determines N , i.e., the number of nodes participating in the determination of the coefficients $\mathbf{a}(\mathbf{x})$. The smoothness of the resulting approximation is related to the smoothness of the weight functions [9], thus, the higher order derivatives of the approximation have discontinuities at the border of the influence regions of the nodes when radial basis functions or truncated Gaussian functions are used as weight functions [10], [17]. We propose to use smooth, i.e., C^∞ , weight functions in order to obtain a smooth approximation. The smooth functions we use are

$$w_j(\mathbf{x}) = \begin{cases} e^{-\lambda_j/(1-(|\mathbf{x}-\mathbf{x}_j|/r_j)^2)}, & |\mathbf{x} - \mathbf{x}_j| \leq r_j \\ 0, & |\mathbf{x} - \mathbf{x}_j| \geq r_j \end{cases} \quad (8)$$

where λ_j controls the rate the weight function tends to zero.

Equation (7) poses a moving (due to its dependence on \mathbf{x}) least-squares problem for the vector \mathbf{a} . Defining $P = [\mathbf{p}(\mathbf{x}_1), \dots, \mathbf{p}(\mathbf{x}_N)]^T$ and $W(\mathbf{x}) = \text{diag}\{w_1(\mathbf{x}), \dots, w_N(\mathbf{x})\}$, where $\text{diag}\{\dots\}$ is a diagonal matrix with the given elements on the main diagonal, we get the following well-known solution

$$\mathbf{a}(\mathbf{x}) = (P^T W(\mathbf{x}) P)^{-1} P^T W(\mathbf{x}) \tilde{\Phi} \quad (9)$$

where $\tilde{\Phi} = [\tilde{\Phi}_1, \dots, \tilde{\Phi}_N]^T$. In order to obtain a unique least-squares solution, the point \mathbf{x} must be contained in the influence region of at least K nodes. These nodes cannot be arranged in certain special patterns such as a plane or spherical surface, to preserve the full column rank of the matrix P .

Note that the vector $\tilde{\Phi}$, whose elements are the potentials $\tilde{\Phi}_j$, is not known *a priori* and has to be computed. However, by assuming it was known we were able to get expression (9) for computing \mathbf{a} in (5). To show that we constructed a global approximation for the potential let $\mathbf{u}^T(\mathbf{x}) = \mathbf{p}^T(\mathbf{x})(P^T W(\mathbf{x}) P)^{-1} P^T W(\mathbf{x})$ then, from (5) and (9) we get

$$\Phi^a(\mathbf{x}) = \mathbf{u}^T(\mathbf{x}) \tilde{\Phi} = \sum_{j=1}^N u_j(\mathbf{x}) \tilde{\Phi}_j. \quad (10)$$

The function $u_j(\mathbf{x})$ is called the *shape function* [11] of the node j . We see then that the electric potential approximation at \mathbf{x} is a linear combination of the shape functions associated with nodes whose influence region enclose \mathbf{x} , and the coefficients of this linear combination are contained in the vector $\tilde{\Phi}$.

The shape functions have the same support as the weight functions, they are also smooth, and any linear combination of the functions used as the basis of the local potential approximation can be represented globally without error as a linear combination of the shape functions [9]. Note that since $u_j(\mathbf{x}_i) \neq 0$ for $i \neq j$, this method only approximates the electric potential of the nodes but does not interpolate their value, as BEM or FEM do.

In the following subsections, we will show how to compute the vector $\tilde{\Phi}$ and obtain the global approximation to the solution of the EEG forward problem.

A. Boundary Conditions

Most of the known meshless methods solve the Neumann boundary conditions problems with null normal flux across the surface [10], [15]–[17]. This allows imposing the boundary conditions by forcing the shape functions to satisfy them. The resulting approximation is a linear combination of the shape functions and satisfies the boundary conditions too. This kind of methods are called *domain methods*. But the use of singularity separation explained in Section II means that the normal component of the electric potential gradient across the surfaces changes when the parameters of the source vary. Since we plan to use the method for solving the inverse problem, it is important to keep the shape functions independent of the source parameters. With such purpose in mind we introduce in the rest of the section our FPMM, since existing meshless methods do not handle this situation satisfactorily.

The method is mixed because neither the boundary conditions nor the differential equation over the domain are satisfied exactly, in fact only a *weak* weighted residuals integral formulation of the boundary conditions can be satisfied [20]. Since we only know a set of points on the surfaces, it is natural to use a point collocation technique [16]. The solution of the weak integral formulation of the boundary conditions by point collocation is equivalent to evaluating the boundary conditions of (3) on the surface nodes. From (10) an expression is found for the approximation to the normal component of the potential gradient at any point \mathbf{x} on a surface

$$\nabla \Phi^a(\mathbf{x}) \cdot \mathbf{n} = \sum_{j=1}^N \nabla u_j(\mathbf{x}) \cdot \mathbf{n} \tilde{\Phi}_j. \quad (11)$$

Now (3) can be evaluated for every surface node by means of (10) and (11). For any node this involves the coefficients $\tilde{\Phi}$ of the neighboring nodes, yielding the following linear systems for each layer:

$$\Phi = U_S \tilde{\Phi} \quad (12)$$

$$\nabla \Phi \cdot \mathbf{n} = F \tilde{\Phi} \quad (13)$$

where $\Phi = [\Phi^a(\mathbf{x}_1), \dots, \Phi^a(\mathbf{x}_{N_S})]^T$, $\tilde{\Phi} = [\tilde{\Phi}_1, \dots, \tilde{\Phi}_{N_T}]^T$, and N_T is the total number of nodes, U_S and F are rectangular

matrices, because the boundary conditions only apply to nodes on the surfaces, a subset of the total nodes.

The true normal component of the electric potential gradient has a jump across the interfaces between layers of different conductivity. But the electric potential approximation is a linear combination of smooth shape functions, and cannot exactly represent this jump in the normal component of the gradient. There are some methods to overcome this difficulty [11], [21], but they assume a certain extra knowledge of the surface in addition to the location of the nodes. We propose to deal with each layer separately, then combine them by imposing the boundary conditions. This approach increases the size of the linear system to be solved, but it leads to a better approximation.

Suppose there are M layers of different conductivities, with N_{S_i} nodes on interface i and N_{I_i} internal nodes in layer i . The external surface nodes of every layer, denoted with the superscript $+$, must be at the same position than the internal surface nodes of the following layer, denoted with the superscript $-$. For each layer i the matrices $U_{S_i} = [U_i^{-T}, U_i^{+T}]^T$ and F_i are computed as described in previous paragraphs. Note that U_1^- is an empty matrix for the first layer has no inner surface, and U_M^+ is necessary for the computation of the potential approximation on the scalp surface, not to impose boundary conditions.

The following systems are assembled to impose the boundary conditions of (3), for $i = 1, \dots, M-1$

$$\begin{aligned} U_i^+ \tilde{\Phi}_i - U_{i+1}^- \tilde{\Phi}_{i+1} &= \mathbf{0} \\ \sigma_i F_i^+ \tilde{\Phi}_i - \sigma_{i+1} F_{i+1}^- \tilde{\Phi}_{i+1} &= (\sigma_{i+1} - \sigma_i) \mathbf{f}_i \\ \sigma_M F_M^+ \tilde{\Phi}_M &= -\sigma_M \mathbf{f}_M \end{aligned} \quad (14)$$

where $\tilde{\Phi}_i = [\tilde{\Phi}_i^{-T}, \tilde{\Phi}_i^T, \tilde{\Phi}_i^{+T}]^T$, and for $i = 1, \dots, M$

$$\mathbf{f}_i = [\nabla \phi_F(\mathbf{x}_1) \cdot \mathbf{n}, \dots, \nabla \phi_F(\mathbf{x}_{N_{S_i}}) \cdot \mathbf{n}]^T, \quad \mathbf{x}_j \in S_i$$

is the normal component of the flux at the N_{S_i} surface nodes of the i th surface.

These equations can be combined in a single system

$$D \tilde{\Phi} = \mathbf{b} \quad (15)$$

where the coefficient vector is $\tilde{\Phi} = [\tilde{\Phi}_1^T, \dots, \tilde{\Phi}_M^T]^T$. The size of the matrix D is $N_S \times N_T$, with $N_S = 2 \sum_{i=1}^{M-1} N_{S_i} + N_{S_M}$ and $N_T = N_S + \sum_{i=1}^M N_{I_i}$. Equation (15) summarizes the boundary conditions for the multilayered problem.

B. Laplace Equation

In this section, we deal with the Laplace differential equation for the electric potential in the domain representing the head. If we compute the Laplacian of the potential approximation based on (10)

$$\nabla^2 \Phi^a(\mathbf{x}) = \sum_{j=1}^N \nabla^2 u_j(\mathbf{x}) \tilde{\Phi}_j \quad (16)$$

it can be seen that since the Laplacian of the shape functions is not zero, neither is the Laplacian from the proposed approximation. Even though the potential approximation $\Phi^a(\mathbf{x})$ does not exactly satisfy the Laplace differential equation in the whole

domain, we can still force it to satisfy a weighted residual integral formulation. Using again a point collocation technique, the evaluation of this integral formulation is equivalent to the evaluation of the first equation of (3) at every node. Writing (16) for all the nodes in each layer $i = 1, \dots, M$, we get the linear systems

$$\sigma_i L_i \tilde{\Phi}_i = \mathbf{0}. \quad (17)$$

Combining them, we obtain the block diagonal system

$$L \tilde{\Phi} = \mathbf{0} \quad (18)$$

where the matrix L is of size $N_T \times N_T$.

C. The Complete Set of Linear Equations System

In the previous two sections we saw that the boundary conditions and the differential equation in the domain are not satisfied exactly, but through a weighted residual integral formulation. This is the reason why the method is called mixed. However, with this formulation (15) and (18) can not be satisfied simultaneously by any vector $\tilde{\Phi}$ because there are more equations than nodes. One possible solution is finding the vector that minimizes the Laplace equation at the nodes, constrained by the boundary conditions, i.e.,

$$\tilde{\Phi} = \min_{D \tilde{\Phi} = \mathbf{b}} \|L \tilde{\Phi}\|. \quad (19)$$

There exist several algorithms to solve this well-known constrained optimization problem [22]. Since the electric potential approximation is computed at each point based only on the nearest nodes, the resulting linear systems are represented by sparse matrices. A good algorithm to solve the numerical problem should take advantage of the matrices' sparsity, for this decreases the computational burden. One possibility is to solve the linear problem

$$H^T H \tilde{\Phi} = D^T \mathbf{b} \quad (20)$$

where $H = [D^T, \epsilon L^T]^T$, with $\epsilon \ll 1$.

Since the EEG forward problem has Neumann boundary conditions, it has an infinite number of solutions differing in a constant value. The MLS scheme used in our FPMM ensures that any linear combination of the functions used as the basis of the local potential approximation can be represented globally without error. Hence the constant function is represented without error in the discretized version and the rank of the matrix H is $N_T - 1$, with a null singular value associated to the constant eigenvector.

It is possible to avoid this rank deficiency by imposing a new restriction on the optimization. This restriction should fix the potential at some point, or the mean potential of any subset of points. The equation for this restriction is obtained from (10) evaluated at the points of interest. Under these conditions (20) is a symmetric positive definite linear system, and a wide range of iterative methods exist for solving it [23], [24]. Note that it is not convenient to compute explicitly the product $H^T H$ since the sparsity could be lost. Also, the value of ϵ in (20) should not be too small in order to avoid numerical instabilities, we obtained good results with $\epsilon = 0.01$.

Once the coefficient vector $\tilde{\Phi}$ is known, (10) gives an expression for the electric potential approximation at any point. The solution to the EEG forward problem at a point $\mathbf{x} \in \Omega$ is then

$$\phi(\mathbf{x}) = \mathbf{u}^T(\mathbf{x})\tilde{\Phi} + \phi_F(\mathbf{x}) \quad (21)$$

with $\mathbf{u}^T(\mathbf{x}) = [u_1(\mathbf{x}), \dots, u_{N_T}(\mathbf{x})]$.

IV. VARIATIONS

In this section, we analyze some variations of our method in order to improve certain aspects of its behavior. The performance of the different versions is analyzed in Section V.

A. Moving or Local Differentiation

Two different approaches can be taken when computing the derivatives of the shape functions needed in (11) and (16). A local approach assumes that the proposed approximation for the electric potential behaves according to (5) where the coefficient vector \mathbf{a} is assumed constant in the neighborhood of \mathbf{x} . We can write then from (9) and (10)

$$\frac{\partial \mathbf{u}^T(\mathbf{x})}{\partial x_i} \approx \frac{\partial \mathbf{p}^T(\mathbf{x})}{\partial x_i} A^{-1}(\mathbf{x}) P^T W(\mathbf{x}) \quad (22)$$

where $A(\mathbf{x}) = P^T W(\mathbf{x}) P$.

We call this approach local differentiation (LD) method as opposed to a moving differentiation (MD) approach that arises when the dependence of vector $\mathbf{a}(\mathbf{x})$ with \mathbf{x} is considered, as given by (9)

$$\begin{aligned} \frac{\partial \mathbf{u}^T(\mathbf{x})}{\partial x_i} &= \frac{\partial \mathbf{p}^T(\mathbf{x})}{\partial x_i} A^{-1}(\mathbf{x}) P^T W(\mathbf{x}) \\ &\quad - \mathbf{p}^T(\mathbf{x}) A^{-1}(\mathbf{x}) \frac{\partial A(\mathbf{x})}{\partial x_i} A^{-1}(\mathbf{x}) P^T W(\mathbf{x}) \\ &\quad + \mathbf{p}^T(\mathbf{x}) A^{-1}(\mathbf{x}) P^T \frac{\partial W(\mathbf{x})}{\partial x_i}. \end{aligned} \quad (23)$$

Comparing (22) with (23) we can see that the LD version is simpler and hence the computation of the matrices D and L is faster for the LD version.

B. Square Linear System (SLS)

In the previous section we solved the forward problem as a linearly constrained optimization, by minimizing the Laplacian of the approximation subject to the boundary conditions.

It is also possible to write a SLS for the forward problem. This can be done simply by forcing the Laplacian to be null only at the internal nodes. In this way, we get an equation for each node; the Laplace equation for the internal nodes and the boundary conditions for the surface nodes.

Let L_I be the matrix formed by the rows of L that correspond to internal nodes, then the coefficients $\tilde{\Phi}$ are obtained as

$$\begin{bmatrix} D \\ L_I \end{bmatrix} \tilde{\Phi} = \begin{bmatrix} \mathbf{b} \\ \mathbf{0} \end{bmatrix}. \quad (24)$$

We will denote this unconstrained version of the method as SLS.

C. Singularity Separation

Compared with the other layers the skull has a low electric conductivity. This causes a shielding effect, hence the potential in the outer layers has a much lower magnitude than the potential generated by the same source in an infinite homogeneous media. The SSM of Section II consisted in computing the relatively small electric potential $\phi(\mathbf{x})$ as the sum of the relatively large $\phi_F(\mathbf{x})$ and the numerically calculated $\Phi(\mathbf{x})$. Hence the latter has opposite signs and tends to cancel $\phi_F(\mathbf{x})$. Then small relative errors in $\Phi(\mathbf{x})$ may cause large relative errors in $\phi(\mathbf{x})$. Thus, for the layers enclosing the skull it may be better to directly compute the potential distribution rather than to use SSM.

If the SSM is applied from the first to k th layers only, the electric potential $\phi(\mathbf{x}) = \Phi(\mathbf{x}) + \phi_F(\mathbf{x})$ for $\mathbf{x} \in \Omega_i, i \leq k$ and $\phi(\mathbf{x}) = \Phi(\mathbf{x})$ for $\mathbf{x} \in \Omega_i, i > k$. Then the boundary conditions on (3) change to

$$\begin{aligned} &\Phi(\mathbf{x}^+) - \Phi(\mathbf{x}^-) \\ &= \begin{cases} 0, & \mathbf{x} \in S_i, i \neq k \\ \phi_F(\mathbf{x}), & \mathbf{x} \in S_k \end{cases} \\ &\sigma_i \nabla \Phi(\mathbf{x}^-) \cdot \mathbf{n} - \sigma_{i+1} \nabla \Phi(\mathbf{x}^+) \cdot \mathbf{n} \\ &= \begin{cases} (\sigma_{i+1} - \sigma_i) \nabla \phi_F(\mathbf{x}) \cdot \mathbf{n}, & \mathbf{x} \in S_i, i < k \\ -\sigma_i \nabla \phi_F(\mathbf{x}) \cdot \mathbf{n}, & \mathbf{x} \in S_k \\ 0, & \mathbf{x} \in S_i, i > k \end{cases}. \end{aligned} \quad (25)$$

These changes in the boundary conditions affect only the vector \mathbf{b} in (15), while the matrix D remains unchanged. Also, when computing the solution to the EEG forward problem with (21), the term ϕ_F should be added only to points located in the layers $i = 1, \dots, k$.

D. Isolated Skull Approach

The electric conductivity of the skull is almost two orders of magnitude smaller than of its neighboring layers. This important discontinuity causes some numerical instability when solving the forward problem. The numerical stability of the results obtained with BEM improves considerably using the isolated skull approach (ISA) [25]. We discuss how to apply this approach to our meshless method.

The ISA solves the forward problem in two stages. First, the problem is solved assuming that the conductivity of the skull is null. Then, the difference between this result and the real electric potential distribution is computed. The complete solution is the sum of these two terms. The idea is that the first problem involves only the layers beneath the skull, for which the results have relatively small errors. The difference with the real solution is small, hence its error is also small.

For the FPMM, first we assume the skull has null conductivity which isolates the outer layers. Hence a reduced size problem must be solved. The vector \mathbf{b}_o and the matrices D_o and L_o are assembled from (14) and (17) with $i = 1, \dots, k - 1$, where k is the skull layer. Let $\tilde{\Phi}_o$ be the vector that minimizes $\|L_o \tilde{\Phi}_o\|$ subject to $D_o \tilde{\Phi}_o = \mathbf{b}_o$, and

$$\phi_o(\mathbf{x}) = \begin{cases} \mathbf{u}^T(\mathbf{x})\tilde{\Phi}_o + \phi_F(\mathbf{x}), & \mathbf{x} \in \Omega_i, i < k \\ \mathbf{0}, & \mathbf{x} \in \Omega_i, i \geq k \end{cases}. \quad (27)$$

Then the full-size problem (19) involving all the layers is solved, but with a different vector \mathbf{b} , given by the modified boundary conditions

$$\Phi(\mathbf{x}^-) - \Phi(\mathbf{x}^+) = \begin{cases} 0, & \mathbf{x} \in S_i, i \neq k-1 \\ \phi_o(\mathbf{x}), & \mathbf{x} \in S_{k-1} \end{cases} \quad (28)$$

$$\sigma_i \nabla \Phi(\mathbf{x}^+) \cdot \mathbf{n} - \sigma_{i+1} \nabla \Phi(\mathbf{x}^-) \cdot \mathbf{n} = 0. \quad (29)$$

Let $\tilde{\Phi}$ be the solution of this full-size problem, then the EEG forward problem solution is given by

$$\phi(\mathbf{x}) = \mathbf{u}^T(\mathbf{x})\tilde{\Phi} + \phi_o(\mathbf{x}). \quad (30)$$

V. RESULTS

In this section, we analyze the performance of our method by numerically solving the forward problem for head models with spherical geometry. For these models the forward problem has a known analytical solution [6] we can compare our numerical results to. As a reference, we also compare our meshless method with the frequently used BEM.

To quantify the error we considered two different measures, a normalized relative difference measure (NRDM) that measures the error in the shape of the distribution of the electric potential, and a measure of the electric potential magnitude error (MAG). These measures are frequently used for distributions comparisons [25] and are defined by

$$\text{NRDM} = \left\| \frac{\Phi_a}{\|\Phi_a\|} - \frac{\Phi_n}{\|\Phi_n\|} \right\| \quad (31)$$

$$\text{MAG} = \frac{\|\Phi_n\|}{\|\Phi_a\|} \quad (32)$$

where Φ_a is a vector of analytically computed potentials and Φ_n is a vector of numerically computed potentials, both potentials evaluated in all the nodes on the outermost surface.

From the inverse problem point of view, the MAG is related only to the intensity of the source, whereas the NRDM to its orientation and position. Since the NRDM measure involves five of the six source parameters, we focused our attention on it. The NRDM value varies between 0 and 2, it is null if the vectors are equal, $\sqrt{2}$ if the vectors are orthogonal and 2 if they are equal but with opposite sign.

All the BEM results were obtained using the same surface nodes as with FPMM, where the nodes are the vertices of triangular elements and a linear variation of the potential over the elements is adopted [2]. The results shown in this section correspond to tangentially oriented dipoles. As when solving with BEM, the results for radially oriented ones are similar with a slightly higher error. Each point shown is the mean NRDM of 240 sources uniformly distributed over a sphere at the given depth, with a random angle in the tangential plane.

Since we have a high degree of freedom to choose the internal node positions because there is no need to form regular elements, we chose the easiest way to place them, i.e., in a regular grid with the separation h between internal nodes constant. Random locations for the nodes, with a fixed density, were also tested and do not affect the results significantly.

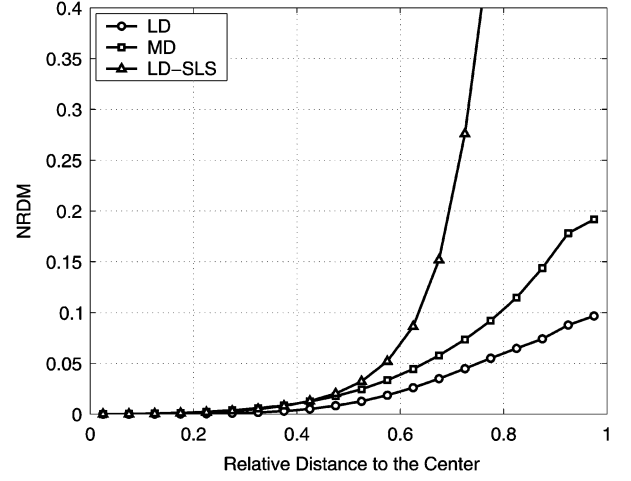


Fig. 2. NRDM as a function of the source depth in a constant conductivity sphere. Results are shown for three variations of our method: LD, MD, and LD-SLS.

In all the examples the radius of the support of each weight function (8) was $r = 2.64h$, such that approximately 81 nodes were included in the influence region of the node, and the parameter λ of the weight function was set to $\lambda = 4$.

In Fig. 2, we show a comparison between different versions of the method for a constant conductivity sphere of radius r_1 . The distance between nodes was set to $h = .12r_1$, and 642 nodes were placed on the surface of the sphere. The figure shows the NRDM as a function of the distance from the source to the center of the sphere. It can be seen that the LD version performs better than the MD version.

Fig. 2 also shows the performance of the forward problem when solved with a SLS. The performance of this version is very poor for sources near the surfaces. This is not surprising since the Laplacian is not minimized at the surface nodes. Since the multilayered EEG problem has thin layers the SLS version will not perform adequately.

The remaining results shown in this section were obtained for a three layered sphere with conductivities $\sigma_1 = \sigma_3 = 80\sigma_2$ and radii $r_3 = 1.15r_1, r_2 = 1.06r_1$. The spherical geometry was used because a series is known for the analytical solution [6].

Figs. 3 and 4 show a comparison between our FPMM and BEM based on the NRDM and MAG as a function of the source distance to the center of the spheres relative to r_1 . For BEM two results are shown, with and without ISA, in both cases for 642 nodes per surface. The meshless method has the same surface nodes, but additional interior nodes, with $h = .12r_1$ for the innermost layer and $h = .08r_1$ for the remaining layers. The total number of nodes for the three layers is near 7500.

We can see the results for two FPMM versions, when we use the SSM up to the third surface the error is higher than when we use it up to the first surface, as predicted in Section IV.C. The results for the ISA version of the FPMM are not shown because they are almost identical to the results obtained when SSM is used only in the innermost layer. This could be expected because the SSM already exploits the principle on which the ISA method is based.

Compared with BEM, the performance of FPMM is very good for deep sources, but for sources near the surface of the

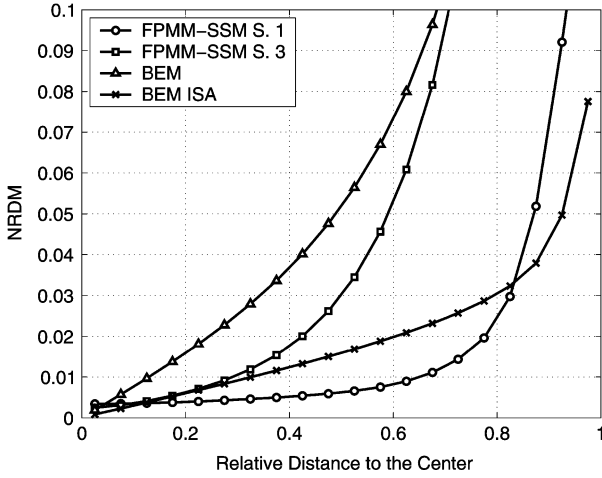


Fig. 3. NRDM as a function of the source depth in a three layered sphere. Comparison between our FPMM with singularity separation up to the first (FPMM-SSM S.1) and third (FPMM-SSM S.3) surfaces and BEM with the isolated skull approach (BEM-ISA) and without it (BEM).

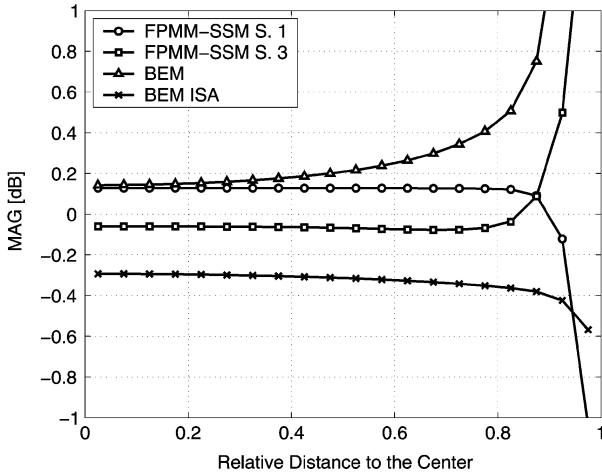


Fig. 4. MAG measure as a function of the source depth in a three layered sphere. Comparison between our FPMM with singularity separation up to the first (FPMM-SSM S.1) and third (FPMM-SSM S.3) surfaces and BEM with the isolated skull approach (BEM-ISA) and without it (BEM).

brain the performance of ISA-BEM is better. Both error measures show this behavior.

Fig. 5 shows the convergence of FPMM. The mean, maximum, and minimum NRDM values are shown for 240 sources regularly distributed over a sphere of radius $0.8r_1$. The observed convergence rate is at least $O(h^2)$. In 1-D and 2-D convergence tests, FPMM also showed $O(h^2)$ convergence. Unlike other meshless methods [13], convergence is achieved with a fixed number of nonzero elements per row of the sparse matrices of the method, i.e., with a constant value of N in (7).

We also compared the convergence rate between the meshless method and ISA-BEM, in Fig. 6. It shows the NRDM as a function of the number of nodes per surface, for tangentially oriented sources placed on spheres at depth $0.6r_1$ and $0.8r_1$. We can see that the convergence rate for FPMM is higher than for BEM. We emphasize that this comparison was made for the same number and location of surface nodes. The total nodes are 246, 486, 966, and 1926 for BEM and 805, 1700, 3575, and 7560 for FPMM.

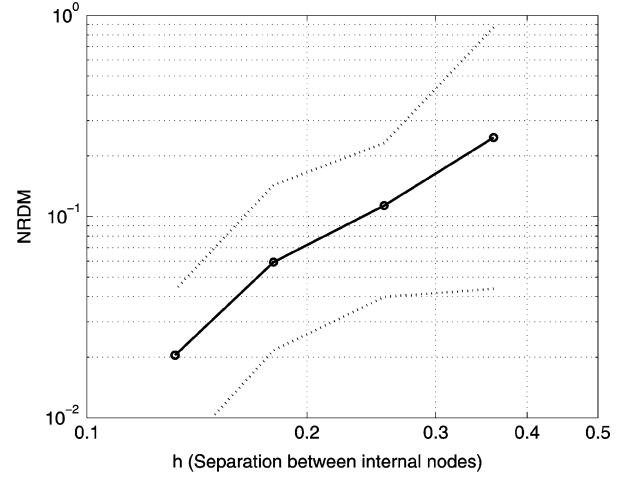


Fig. 5. Convergence of the FPMM. NRDM as a function of the separation between neighboring internal nodes. Results correspond to dipoles located at a constant depth in a three layered spherical head model. The maximum and minimum error for 240 dipoles are shown as dotted lines, the mean error as a full line.

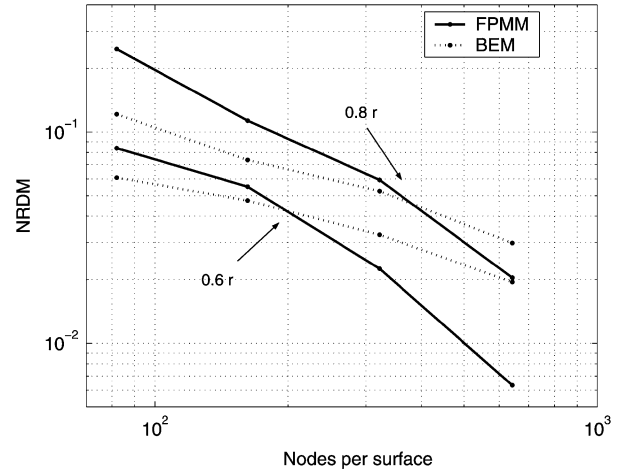


Fig. 6. Convergence comparison between FPMM and BEM. NRDM as a function of the number of nodes per surface in a three layered spherical head model. The figure shows the error for sources at two different depths.

Analysis of the computational complexity of our method indicates that the operation count for assembling the matrices is $O(N_T)$, where N_T is the total number of nodes. The memory needed to store the matrices is $O(N_T)$, and the operation count for solving (20) consists in a few iterations each of order $O(N_T)$. Also, a proper preconditioner should be computed [23], [24]. This can involve a large number of operations, but needs to be done only once if many forward problems must be solved, e.g., when solving the inverse problem. Note that for BEM the operation count is $O(N_S^2)$ for the assembling of the matrix and solution to one forward problem, although the number of operations could be lowered according to recent results [26], [27].

The total number of nodes N_T is related to the distance h between neighboring nodes as $h \sim N_S^{-2}$ for BEM, and for FPMM $h \sim N_T^{-3}$ in the worst case (when h is small enough as to make the number of boundary nodes negligible compared to the total number of nodes). If we want to reduce h by a factor two, FPMM

would increase 8 times the operation count for assembling the matrices and the memory needed to store them, and the error in the solution of the forward problem would be reduced by a factor 4. In contrast, for BEM the number of nodes would increase 4 times, the operation count for assembling the matrix would increase 16 times, just as the memory needed to store it, while the error would be reduced by a factor smaller than FPMM's 4.

VI. DISCUSSION

We presented a numerical FPMM for solving the EEG forward problem in bodies of piecewise constant conductivity and arbitrary shape. The method uses both surface and volume nodes but does not need a mesh connecting the nodes of the problem. This can save the typically computationally expensive generation of these meshes for BEM and FEM in 3-D problems, especially for the intricate shapes involved in the layers for the EEG and related problems.

From our comparisons with the widely used BEM, it is clear that our FPMM needs more nodes to achieve solutions with the same precision. This could have been predicted since BEM needs only surface nodes, roughly lowering the dimension of the problem by one. On the other hand, the matrix related to FPMM is sparse, whereas the BEM matrices are full. This amounts to important savings in time, storage requirements and in the number of operations needed to assemble the matrices associated with the problem. Our results indicate that for a few thousands nodes per surface, as in the usual descriptions of the head surfaces used in BEM [7], the error of FPMM and BEM are of the same order, whereas the operation count to solve the forward problem is lower for BEM. These results also suggest that for problems with a higher number of nodes (e.g., in surface descriptions including the sulci and fissures of the cortical layer) the FPMM would need less operations than BEM for solving the forward problem with similar precision. These savings become significant in view of the ever increasing number of nodes being used as the demand for precision increases. When the inverse problem involves many consecutive computations of the direct problem, the savings in the computational effort obtained with our FPMM become an important advantage.

For problems with a limited number of nodes the method also produces good results and could be used in EEG related problems. In fact, our FPMM allows a simple computation of the sensitivity of the forward problem solution to perturbations in the geometry of the head model. We used this feature to study the effect of perturbations in the geometry on the EEG inverse problem. Preliminary results of this approach were presented in [28].

The solution of the forward problem with our FPMM involves a minimization with constraints. The search of the numerical algorithm best suited to solve the problem is not the purpose of this paper, although is a topic worth studying. In this paper, we proposed a procedure to solve the problem taking advantage of the sparsity of the matrices involved. However, other choices are possible, and different alternatives may be considered in the search for the best method. For instance, since our FPMM shares many characteristics (such as sparsity and the need of internal nodes) with FEM, it would be interesting to study the use of fast solvers designed for FEM [24] to solve (19).

Finally we would like to point out that although the method was designed to solve specifically the EEG forward problem, it could be used with little modifications to solve other partial differential equations problems with boundaries known only at a finite set of points.

REFERENCES

- [1] M. S. Hamäläinen and J. Sarvas, "Realistic conductivity geometry model of the human head for interpretation of neuromagnetic data," *IEEE Trans. Biomed. Eng.*, vol. 36, no. 2, pp. 165–171, Feb. 1989.
- [2] J. C. de Munck, "A linear discretization of the volume conductor boundary integral equation using analytically integrated elements," *IEEE Trans. Biomed. Eng.*, vol. 39, no. 9, pp. 986–990, Sep. 1992.
- [3] A. van Oosterom and J. Strackee, "The solid angle of a plane triangle," *IEEE Trans. Biomed. Eng.*, vol. 30, no. 2, pp. 125–126, Feb. 1983.
- [4] Y. Yan, P. L. Nunez, and R. T. Hart, "Finite-element model of the human head: Scalp potentials due to dipole sources," *Meth. Biol. Eng. Comput.*, vol. 29, pp. 475–481, Sep. 1991.
- [5] S. P. van den Broek, H. Zhou, and M. J. Peters, "Computation of neuro-magnetic fields using finite-elements method and Biot-Savart law," *Med. Biol. Eng. Comput.*, vol. 34, pp. 21–26, Jan. 1996.
- [6] J. C. de Munck and M. J. Peters, "A fast method to compute surface potentials in the multisphere model," *IEEE Trans. Biomed. Eng.*, vol. 40, no. 11, pp. 1166–1174, Nov. 1993.
- [7] D. van't Ent, J. C. de Munck, and A. L. Kaas, "A fast method to derive realistic BEM models for E/MEG source reconstruction," *IEEE Trans. Biomed. Eng.*, vol. 48, no. 12, pp. 1434–1443, 2001.
- [8] S. N. Atluri and S. Shen, "The meshless local Petrov-Galerkin (MLPG) method: A simple & less-costly alternative to the finite element and boundary element methods," *Comput. Model. Eng. Sci.*, vol. 3, no. 1, pp. 11–51, 2002.
- [9] I. Babuška and J. M. Melenk, "The partition of unity method," *Int. J. Numer. Meth. Eng.*, vol. 40, pp. 727–758, 1997.
- [10] T. Belytschko, P. Krysl, and Y. Krongauz, "A three-dimensional explicit element-free Galerkin method," *Int. J. Numer. Meth. Fluids*, vol. 24, pp. 1253–1270, 1997.
- [11] T. Belytschko, Y. Krongauz, D. Organ, M. Fleming, and P. Krysl, "Meshless methods: An overview and recent developments," *Comput. Method. Appl. Mech. Eng.*, vol. 139, pp. 3–47, 1996.
- [12] C. A. M. Duarte and J. T. Oden, "Hp clouds—An hp meshless method," *Numer. Meth. Partial Diff. Eqs.*, vol. 12, pp. 673–705, 1996.
- [13] G. E. Fasshauer, "Solving differential equations with radial basis functions: Multilevel methods and smoothing," *Adv. Comput. Math.*, vol. 11, pp. 139–159, 1999.
- [14] Y. X. Mukherjee and S. Mukherjee, "The boundary node method for potential problems," *Int. J. Numer. Meth. Eng.*, vol. 40, pp. 797–815, 1997.
- [15] B. Nayroles, G. Touzot, and P. Villon, "Generalizing the finite element method: Diffuse approximation and diffuse elements," *Comput. Mech.*, vol. 10, pp. 307–318, 1992.
- [16] E. Oñate, S. Idelsohn, O. C. Zienkiewicz, and R. L. Taylor, "A finite point method in computational mechanics. Applications to convective transport and fluid flow," *Int. J. Numer. Meth. Eng.*, vol. 39, no. 22, pp. 3839–3886, 1996.
- [17] T. Zhu, J.-D. Zhang, and S. N. Atluri, "A local boundary integral equation (LBIE) method in computational mechanics, and a meshless discretization approach," *Comput. Mech.*, vol. 21, pp. 223–235, 1998.
- [18] J. C. de Munck, B. W. van Dijk, and H. Spekreijse, "Mathematical dipoles are adequate to describe realistic generators of human brain activity," *IEEE Trans. Biomed. Eng.*, vol. 35, no. 11, pp. 960–966, Nov. 1988.
- [19] J. D. Jackson, *Classical Electrodynamics*, 2nd ed. New York: Wiley, 1975.
- [20] B. Jiang, *The Least-Squares Finite Element Method. Theory and Applications in Computational Fluid Dynamics and Electromagnetics*, ser. Scientific Computation. New York: Springer, 1998.
- [21] C. Hérault and Y. Maréchal, "Boundary and interface conditions in meshless methods," *IEEE Trans. Magn.*, vol. 35, no. 3, pp. 1450–1453, May 1999.
- [22] C. L. Lawson and R. J. Hanson, *Solving Least Squares Problems*, ser. Automatic Computation. Upper Saddle River: Prentice-Hall, 1974.
- [23] A. George and J. W. H. Liu, *Computer Solutions of Large Sparse Positive Definite Systems*. Upper Saddle River: Prentice-Hall, 1981.
- [24] I. S. Duff, "Sparse numerical linear algebra: Direct methods and preconditioning," in *The State of the Art in Numerical Analysis*, I. S. Duff and G. A. Watson, Eds. Oxford, U.K.: Oxford Univ. Press, 1997, pp. 27–62. [Online]. Available: citeseer.ist.psu.edu/duff96sparse.html.

- [25] J. W. H. Meijs, O. W. Weier, M. J. Peters, and A. van Oosterom, "On the numerical accuracy of the boundary element method," *IEEE Trans. Biomed. Eng.*, vol. 36, no. 10, pp. 1038–1049, Oct. 1989.
- [26] N. Krzobek and S. Sauter, "Fast Cluster Techniques for BEM," Univ. Zurich, Zurich, Switzerland, [Online]. Available: <http://www.math.unizh.ch/fileadmin/math/preprints/04-02rev.pdf>, 2002.
- [27] G. Alléon, M. Benzi, and L. Giraud, "Sparse approximated inverse preconditioning for dense linear systems arising in computational electromagnetics," *Numer. Algorithms*, vol. 16, no. 1, pp. 1–15, 1997.
- [28] N. von Ellenrieder, C. H. Muravchik, and A. Nehorai, "Effect of perturbations in the geometry on the EEG inverse problem," in *Proc. 2003 IEEE Workshop Statistical Signal Processing*, Oct. 2003, pp. 273–276.



Nicolás von Ellenrieder (S'01) was born in Argentina, April 27, 1975. He graduated in 1998 as an Electronics Engineer from the National University of La Plata, La Plata, Argentina, where he is working towards the Ph.D. degree.

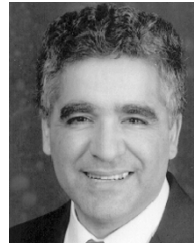
He is an Assistant Lecturer at the Department of the Electrical Engineering of the National University of La Plata and a member of its Industrial Electronics, Control and Instrumentation Laboratory (LEICI). His research interests include statistical processing of biomedical signals.



Carlos H. Muravchik (S'81–M'83–SM'99) was born in Argentina, June 11, 1951. He graduated as an Electronics Engineer from the National University of La Plata, La Plata, Argentina, in 1973. He received the M.Sc. in statistics (1983) and the M.Sc. (1980) and Ph.D. (1983) degrees in electrical engineering, from Stanford University, Stanford, CA.

He is a Professor at the Department of the Electrical Engineering of the National University of La Plata and a member of its Industrial Electronics, Control and Instrumentation Laboratory (LEICI). He is also a member of the Comisión de Investigaciones Científicas de la Pcia. de Buenos Aires. He was a Visiting Professor at Yale University, New Haven, CT, in 1983 and 1994, and at the University of Illinois at Chicago in 1996, 1997, 1999, and 2003. His research interests are in the area of statistical signal and array processing with biomedical, control, and communications applications, and nonlinear control systems.

Since 1999, Dr. Muravchik is a member of the Advisory Board of the journal *Latin American Applied Research* and is currently an Associate Editor of the *IEEE TRANSACTIONS ON SIGNAL PROCESSING*.



Arye Nehorai (S'80–M'83–SM'90–F'94) received the B.Sc. and M.Sc. degrees in electrical engineering from the Technion, Haifa, Israel, and the Ph.D. degree in electrical engineering from Stanford University, Stanford, CA.

After graduation he worked as a Research Engineer for Systems Control Technology, Inc., in Palo Alto, CA. From 1985 to 1989, he was Assistant Professor and from 1989 to 1995 he was Associate Professor with the Department of Electrical Engineering at Yale University, New Haven, CT. In 1995,

he joined the Department of Electrical Engineering and Computer Science at The University of Illinois at Chicago (UIC), as a Full Professor. From 2000 to 2001, he was Chair of the department's Electrical and Computer Engineering (ECE) Division, which is now a new department. In 2001, he was named University Scholar of the University of Illinois. He holds a joint professorship with the ECE and Bioengineering Departments at UIC. His research interests are in signal processing, communications, and biomedicine.

Dr. Nehorai is Vice President-Publications and Chair of the Publications Board of the IEEE Signal Processing Society. He is also a member of the Board of Governors and of the Executive Committee of this Society. He was Editor-in-Chief of the *IEEE TRANSACTIONS ON SIGNAL PROCESSING* from January 2000 to December 2002, and is currently a Member of the Editorial Board of *Signal Processing*, the *IEEE Signal Processing Magazine*, and *The Journal of the Franklin Institute*. He is the founder and Guest Editor of the special columns on Leadership Reflections in the *IEEE Signal Processing Magazine*. He has previously been an Associate Editor of *IEEE TRANSACTIONS ON ACOUSTICS, SPEECH, AND SIGNAL PROCESSING*, *IEEE SIGNAL PROCESSING LETTERS*, the *IEEE TRANSACTIONS ON ANTENNAS AND PROPAGATION*, *IEEE JOURNAL OF OCEANIC ENGINEERING*, and *Circuits, Systems, and Signal Processing*. He served as Chairman of the Connecticut IEEE Signal Processing Chapter from 1986 to 1995, and a Founding Member, Vice-Chair, and later Chair of the IEEE Signal Processing Society's Technical Committee on Sensor Array and Multichannel (SAM) Processing from 1998 to 2002. He was the co-General Chair of the First and Second *IEEE SAM Signal Processing Workshops* held in 2000 and 2002. He was co-recipient, with P. Stoica, of the 1989 IEEE Signal Processing Society's Senior Award for Best Paper, and co-author of the 2003 Young Author Best Paper Award of this Society, with A. Dogandzic. He received the Faculty Research Award from the UIC College of Engineering in 1999 and was Adviser of the UIC Outstanding Ph.D. Thesis Award in 2001. He was elected Distinguished Lecturer of the IEEE Signal Processing Society for the term 2004 to 2005. He has been a Fellow of the Royal Statistical Society since 1996.